environmental and earth sciences proceedings

MDPI

Proceeding Paper

The Influence of Mechanochemical Synthesis Method on Photodegradability Characteristics of Hydroxyapatite/Zinc Oxide Composite †

Cristina Rodica Dumitrescu, Florina-Diana Gheorghe *, Monica Matei, Larisa-Mădălina Ștefan and Elena Holban

National Institute for Research and Development in Environmental Protection, 294 Splaiul Independenței Blv, 060031 Bucharest, Romania; cristinadumitrescu0@gmail.com (C.R.D.); monicamatei06@gmail.com (M.M.); lara_madalina@yahoo.com (L.-M.Ș.); elena.holban@incdpm.ro (E.H.)

* Correspondence: dianadumitru1986@gmail.com

† Presented at the 6th International Conference on Green Environmental Engineering and Technology (IConGEET2024), Bali, Indonesia, 29–30 August 2024.

Abstract: The ZnO/hydroxyapatite nanocomposite was prepared by attrition in a planetary mill from hydroxyapatite (HA) and ZnO nanopowders. The photocatalytic degradation of synthetic dye, methyl orange (MO), was evaluated under stirring and UV irradiations by measuring the spectroscopically UV-VIS absorbance of the solution in order to determine the remanent dye concentration. The samples CZH3 (75% ZnO) and CZH4 (25% ZnO) highlighted the best MO retention from aqueous solution by adsorption and photodegradation effects. The high absorbance of the proposed nanocomposites showed their potential to be used as photocatalysts for wastewater treatment to enable the retention of organic pollutants.

Keywords: composites; photocatalysis; zinc oxide; hydroxyapatite; adsorption; water pollution

Academic Editor: Sara Yasina Yusuf

Published: 18 February 2025

Citation: Dumitrescu, C.R.; Gheorghe, F.-D.; Matei, M.; Ștefan, L.-M.; Holban, E. The Influence of Mechanochemical Synthesis Method on Photodegradability Characteristics of Hydroxyapatite/Zinc Oxide Composite. *Environ. Earth Sci. Proc.* **2025**, *33*, 3. https://doi.org/10.3390/eesp2025033003

1. Introduction

Wastewater has a complex composition due to being collected from different sources like domestic, industrial, commercial, or agricultural ones and it contains many harmful organic pollutants such as dyes, drugs, and also heavy metals in the form of a mixture of pollutants [1]. In addition, conventional drainage systems are unable to manage the increased discharges brought on by rapid urbanization. Low Impact Development practices are emerging as innovative concepts to simulate wastewater discharges prior to development, but water pollutant mixture monitoring is still a problem [2,3].

The treatment of pigments or pharmaceutical residues in wastewater is generally inefficient, expensive, and non-destructive, and it transfers the pollution from wastewater to another phase, such as the contaminated filter systems utilized for water treatment [4–6]. Heterogeneous photocatalysis methods were reported as more promising technologies for the removal of organic micropollutants [7–9]. The phenomena occur during an advanced oxidation process (AOP) that leads to the formation of primary oxidizing species (e.g., hydroxyl radicals), which will later oxidize the organic/inorganic contaminants in water, generating pollutant degradation [10]. The heterogeneous photocatalysis activity of a material is deeply determined by the adsorption (physisorption and chemisorption) process [11]. In this context, ZnO is considered an alternative to TiO_2 for the photodegradation of surrounding organic pollutants and expressed antibacterial properties, with its compact

crystalline structure revealing modest adsorptive capacities. Therefore, its association with hydroxyapatite (HA), with its fluffy crystal lattice structure, could substantially improve the sorbent properties of the composite [6]. Overall, the nanoparticles of hydroxyapatite have been intensively studied for medical applications but also for adsorption or heavy metal retention from polluted water due to its crystalline structure (monoclinic space groups P21/b and hexagonal P63/m) that allows multiple cations substitutions of the two possible positions of Ca (I) and Ca (II). Also, its structure allows for the incorporation of other groups, such as tetrahedral phosphate positions PO_4^{3-} and channel OH^- ion sites, modifying the various parameters (lattice parameters, crystallinity, crystal dimensions, surface texture), and, subsequently, their properties (i.e., solubility, spectral properties, and thermal stability) [12]. Due to the anionic positions of the hydroxyapatite lattice structure, this material possesses special and natural organic (protein) adhesion abilities, highlighted especially in medical applications, considering only the fact that the bone tissue of vertebrates is a composite material with hydroxyapatite and collagen as main components [13]. Recently, some authors stated that the photocatalytic phenomenon in HA is caused by photoinduced electronic excitation, linked to oxygen vacancies, that leads to the formation of radicals. These radicals can react with water and other ions and help oxidize pollutant molecules [14].

As a result of the efficient recombination of electron–hole pairs in zinc oxide (ZnO), it can absorb a larger percentage of UV light. Wurtzite, the stable phase of zinc oxide, is composed of a hexagonal close-packed arrangement of O^{2-} anions, with Zn^{2+} cations occupying half of the tetrahedral sites, while the remaining half and all of the octahedral sites are left empty [15,16].

In the context of photocatalytic materials, most references described the HA/ZnO composites that were prepared mainly by mixing the two components in the wet phase, followed by hydrothermal treatments [17,18]. Thus, the prepared composite scaffolds will lose the extraordinary specific surface area conferred by the dispersed nanoparticles, leading to a reduction in the sorbent capacity [8]. The process parameters during attrition (process temperature and duration, collision energy, molar ratio of precursor/powder, mixture-to-ball ratio) determine the particle size and distribution of the developed material [19,20].

The main purpose of this paper was to obtain a composite that combines the adsorptive, organic molecules adhesion of ionic nature and weak photoactive properties of HA nanoparticles with the proven photocatalyst properties of ZnO powder. The synthesis of the composite by attrition aims at a very homogeneous distribution of the component powders, the increase in the specific surface area, and the creation of structural defects to enhance the retention and degradation of organic pollutants (OPs).

2. Materials and Methods

2.1. Materials Used for the Development of Hydroxyapatite/Zinc Oxide Composite

The two components used for the development of the composite have been synthesized separately. The hydroxyapatite (HA) synthesis was prepared by coprecipitation starting with eggshells as a calcium source and an aqueous solution with 38.5% of dibasic ammonium phosphate $(NH_4)_2H(PO_4)$ (Sigma Aldrich, Schnelldorf, Germany) as the phosphate precursor. The obtained hydroxyapatite precipitate with a Ca/P ratio of 1.67 was maturated at room temperature for 48 h, cleaned with distilled water (until the pH was 7), and then dried at a temperature of 60 °C. For the synthesis of ZnO nanoparticles, zinc acetate dihydrate $Zn(CH_3CO_2)_2 \cdot 2H_2O$ (Merck, Darmstadt, Germany) diluted in methanol was precipitated with 0.2 M NaOH solution (Merck, Darmstadt, Germany), in a basic reaction medium (pH around 10), under continuous magnetic stirring. The obtained mixture was subjected to hydrothermal treatment under autogenous pressure for 8 h at 125 °C. The

obtained precipitate was cleaned with methanol and then dried at a temperature of 60 °C. The detailed synthesis of both HA and ZnO has been described elsewhere [21,22].

As shown in Table 1, the composites were developed by combining ZnO with HA in various mass ratios. The weighed nanopowders were added to ethanol and ball milled for 0.5 h at 400 rpm, and, subsequently, the obtained suspensions were dried at a temperature of 60 °C. In order to carry out a comparative evaluation, the precursor nanopowders (HA and ZnO) were also included in the laboratory testing.

Table 1. Samples denomination.

Sample Code	ZnO [%]	HA [%]
CHZ1	100	0
CHZ2	0	100
CHZ3	75	25
CHZ4	25	75
CHZ5	50	50

2.2. Methods

The degradation efficiency of MO has been employed to assess the composites' photocatalytic activity. For this purpose, a laboratory experimental assembly that featured a UV lamp (Biocomp LBA 30 W, Iași, Romania, with λmax = 253.7 nm), a magnetic stirrer, a timer, and glass vessels was used. The MO dye solution was prepared (0.0125 mM) and preliminary tests were performed to determine its stability to UV light in the absence of the photocatalyst, indicating that UV does not directly break down the dye. The tests began when 1 g of material was added to a glass vessel that contained 250 mL MO solution, and the samples were kept in the dark for 0.5 h to achieve the adsorption/desorption equilibrium. After exposing the samples to UV light for different periods (0.5 h, 1 h, 2 h, 3 h, and 4 h), 10 mL of each tested sample was collected and centrifuged. The absorbance of MO for each sample was measured using Jenway's UV–VIS absorption spectroscopy (Jenway, Essex, UK) at a wavelength of λ = 460 nm (maximum absorption for MO).

To determine the residual concentration of MO in the tested samples at different time intervals, the Beer–Lambert law was used, as it highlights a dependence between the absorption of UV light and the properties of a material, as can be seen from Equation (1) [23]:

$$A = \varepsilon b C \quad (1)$$

where A is absorbance, ε is molar absorptivity, b is distance between the sample and UV light, and C is concentration. In the case of methyl orange solution, the molar absorptivity is 25,100 $M^{-1}cm^{-1}$ [23], and b is 1 cm (diameter of the spectrophotometer cuvette).

The photocatalytic degradation of the analyzed organic pollutant can be described by the first-order kinetic law according to the Langmuir–Hinshelwood equation (Equation (2)) [24]:

$$ln\frac{C_0}{C} = kt \quad (2)$$

where k is apparent photodegradation rate constant, C_0 is initial concentration of the solution, t is duration of irradiation, and C is concentration of the solution after a certain time t.

The presence of MO dye absorbed on the composite specimens was determined by X-Ray Diffraction (XRD) using D8 Advance (Bruker AXS GmbH, Karlsruhe, Germany) and the DIFFRAC.SUIT measurement software (version 4.6). The spectrum for each analyzed sample was analyzed for 2θ between 10 and 80°.

In order to determine the MO dye retention capacity on the composite nanopowders, thermogravimetric analysis and differential scanning calorimetry were used (Jupiter STA449 F5, Nitzsch, Selb, Germany), through the mass loss recorded when the temperature increased from 25 °C to 550 °C, in N_2 controlled atmosphere.

3. Results and Discussion

The photocatalytic activity of the composite samples was compared with the nanometric powder samples of the components, ZnO and HA, denoted as CHZ1 and CHZ2. The UV irradiation times performed were set at 0.5, 1, 2, 3, and 4 h. The experiment started by keeping the samples in the dark, under continuous magnetic homogenization for 0.5 h to allow sufficient contact between the aqueous solution loaded with the organic pollutant and the adsorbent powders, avoiding the UV degradation process.

In Figure 1, the variation in the MO concentration in the residual aqueous solution after different irradiation durations can be seen, which was calculated using Equation (1). It is observed that the highest concentration of MO after all irradiation times is attributed to the composite CHZ2 with 100% HA content, with values decreasing faster in the first 0.5 h and then slowly. When compared to CHZ1, the sample with 75% ZnO content (CHZ3) had the best results for the residual concentration of the MO solution, followed by the sample with 25% ZnO (CHZ4). Therefore, after 0.5 h UV irradiation time, the sample CHZ4 exhibited the lowest MO residual concentration of 2.613×10^{-5} mol/L, followed by the higher concentration of CHZ3 (3.087×10^{-5} mol/L), 4.103×10^{-5} mol/L for CHZ4 and CHZ5 with 4.665×10^{-5} mol/L. Until 4 h UV irradiation time, all the MO residual concentrations progressively decreased under 0.086×10^{-5} mol/L (CHZ5) for all samples. As expected, the sample CHZ2 kept the highest value of 4.274×10^{-5} mol/L, showing a decrease in MO degradation rate of only 22.2% after four hours of UV irradiation, compared with 99.96%. This result can be explained by the fact that Zn^{2+} substitution of calcium positions in HA is favored by the attrition process during synthesis, causing an increase in the reactive catalytic surface, from active sites on ZnO particles extended at hydroxyapatite ones [20]. On the other hand, the HA powder, containing nanosized particles, has a larger contribution to the MO adsorption compared with ZnO and a special organic molecules adhesion. In addition, the adsorption on the catalyst surface of a larger amount of MO dye leads to the blocking of the active photodegradation centers and therefore a lower degree of degradation, which explains the very good results in the case of samples CHZ4 and CHZ5.

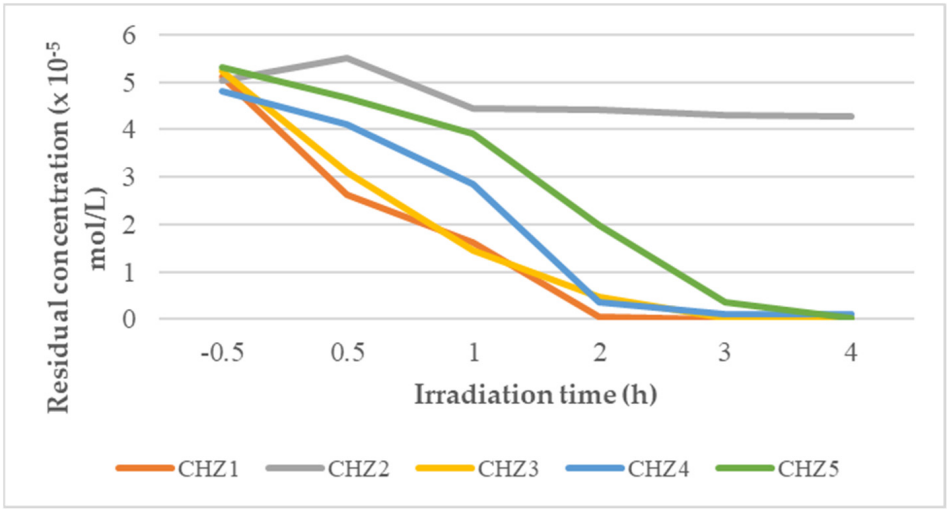

Figure 1. The variation in the MO concentration in the residual aqueous solution during the irradiation time.

However, the photocatalytic activity of sample CHZ1 comes to an end after 2 h of irradiation (the MO concentration is 0.055 compared to 0.001 at 4 h). All the samples reach the minimum MO residual concentration values of <0.086 (99.98%) after 4 h, so the extending of irradiation time will cause insignificant changes in the degree of degradation.

The regression coefficients (R^2) are described in Table 2, and the apparent reaction rate constants (k) are determined from the slopes of the lines in the graphic representations of $\ln(C_0/C)$ as a function of the irradiation time (Equation (2)) from Figure 2. The obtained high values of regression coefficients (R^2), as can be seen in Table 2 for the three composite materials (CHZ3, CHZ4, and CHZ5), indicate that the MO photodegradation mechanism follows Langmuir–Hinshelwood type kinetics. It is also observed that for each analyzed material, the kinetics proceeds with a different constant rate. The photodegradation of the MO solution proceeds at a higher speed for CHZ3 compared to the other composites, which, due to the lower content of ZnO, can more quickly occupy the active sites on the surface of the grains with the massive organic (MO) molecules.

Table 2. Calculated values of apparent photodegradation rate constant (k) and regression coefficient (R^2) as a function of catalyst concentration.

Sample Code	k (h^{-1})	R^2
CHZ1	1.9356	0.9836
CHZ2	0.0483	0.7778
CHZ3	1.5493	0.9593
CHZ4	1.0862	0.9665
CHZ5	1.0013	0.9161

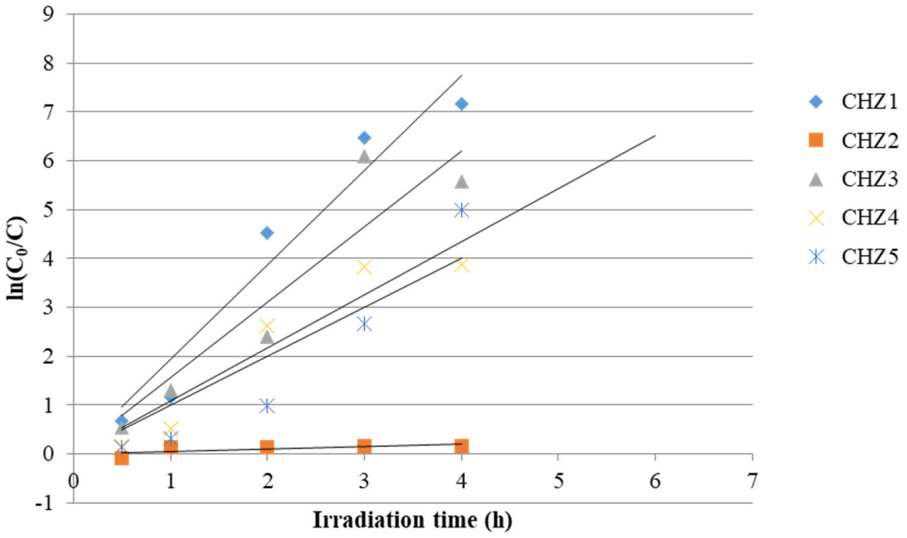

Figure 2. First-order kinetics of the photocatalytic degradation of MO.

The thermogravimetric analysis was used to determine the concentrations of methyl orange adsorbed on the composite powders after different periods of UV irradiating times (Figure 3). Close and low mass loss values were observed for all samples between 150 and 550° C (Figure 3). Also, Figure 3 shows that MO degrades under temperature-increasing conditions up to 550 °C in a reducing environment (N_2), forming carbon (62% of the initial powder quantity) in three steps by eliminating adsorbed water, structurally bound water, and volatile organic compounds or gases (CO_2, NO_x, etc.) resulting from the decomposition of MO. However, samples CHZ3 and CHZ4 show the lowest values of mass losses, 1.31 and 1.78%, respectively, which is explained by the remaining small amounts of adsorbed methyl orange, since the two samples showed the best photodegradation effects. The mass loss of

6.53% for CHZ2 (100% HA) demonstrated that the largest amount of MO was adsorbed on the hydroxyapatite nanoparticle surfaces, without photochemical degradation, with the result being correlated with the highest MO remanent concentration into the CHZ2 solution analyzed after 4 h of irradiation.

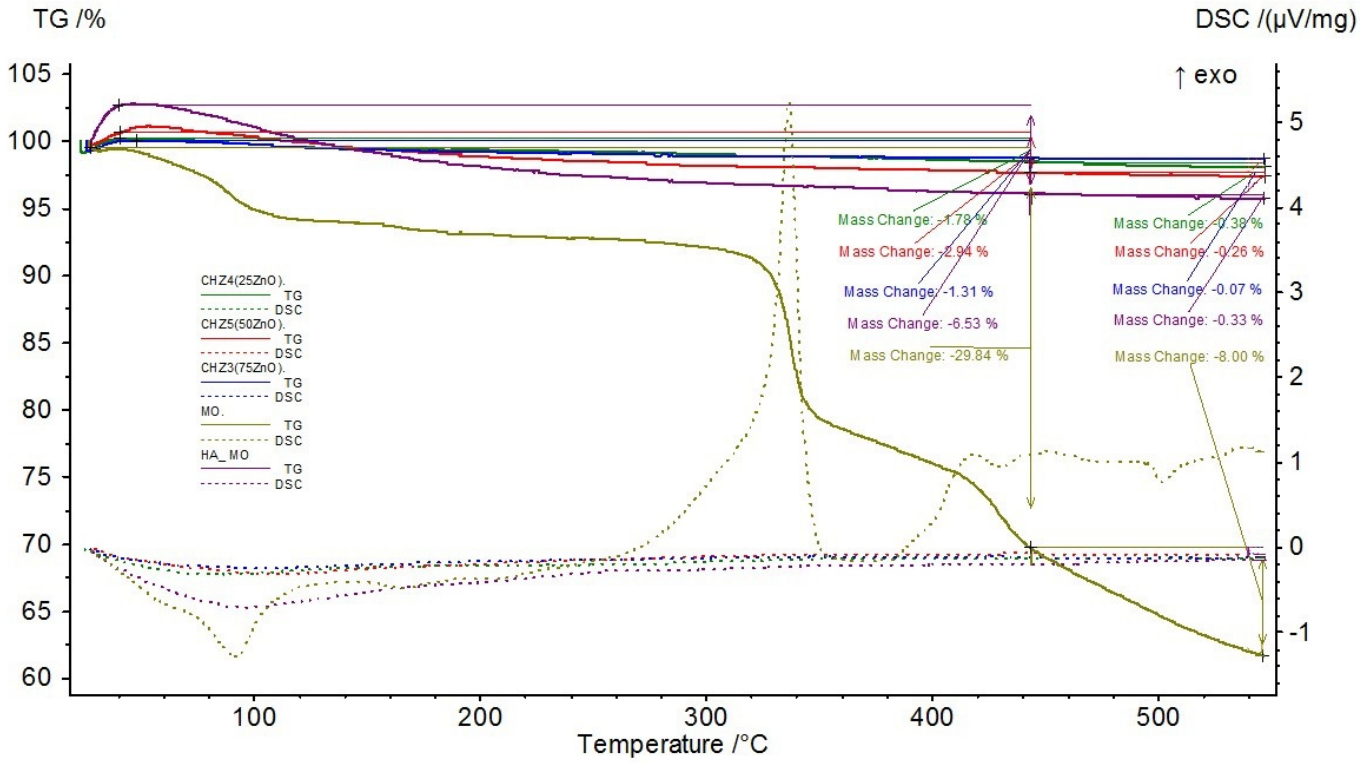

Figure 3. Thermogravimetric and differential scanning calorimetry variation for composite samples after 4 h of UV irradiation time.

X-Ray Diffraction analysis was used to determine the concentrations of remanent methyl orange adsorbed and undegraded on the composite powders (Figure 4). The XRD plots of CHZ3-CHZ5 composite patterns, HA patterns before and after UV irradiation, ZnO before and after UV irradiation, respectively, in Figure 4a, were analyzed comparative and superposed. The characteristic diffraction peaks of methyl orange at 2θ 20.27°, 24.82°, and 27.66° are not found in any of the patterns of the five irradiated powders CHZ1-CHZ5. Only the peak at 2θ 31.65° superposed over the (300) plane of the hexagonal phase of HA powder (2θ 31.77°) and the (100) plane with ZnO hexagonal symmetry (2θ 31.86°). However, the higher degree of crystallinity of the zinc oxide powders (before and after irradiation CHZ1) compared to that of HA, which have a mean crystallite size of 14.69 nm, calculated with the Scherer–Debay formula for the plane (112), is reflected in the diffraction patterns of the CHZ3-CHZ5 composites so that they bear the imprint of the ZnO pattern (Figure 4b). The very low amount of residual MO adsorbed on the analyzed powders is also confirmed by the diffraction plots of HA before and after irradiation (Figure 4c). Comparing the two plots of HA samples, it can be seen that they overlapped almost exactly, without being influenced by the presence of MO crystals adsorbed on HA particle surfaces. The lack of evidence of MO crystals in the XRD patterns of CHZ1-CHZ5 explains the fact that the amounts of dye remaining by adsorption on the powders are very small and cannot be qualitatively determined by this method.

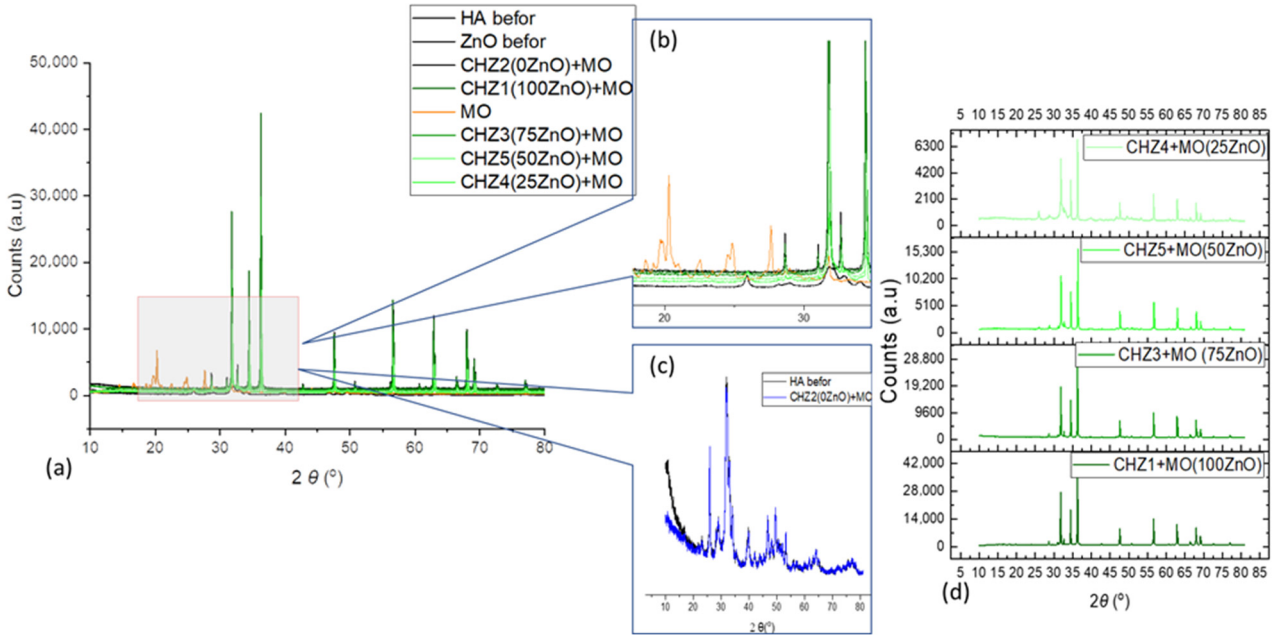

Figure 4. X-Ray Diffraction plot (**a**,**d**) and comparative XRD patterns for composite samples CHZ1-CHZ5 after immersion in MO aq. sol. for 4 h irradiation time, MO dye powder, HA, and ZnO powders before UV treatment; (**b**) insert detail for 2θ 19–35°; (**c**) XRD plot for HA powder before and after immersion for 4 h irradiation time.

4. Conclusions

By using the advanced mechanochemical grinding method for the composite synthesis, three mixtures were obtained with the potential to adsorb organic pollutants due to the increase in the fineness of the two powders. Also, after the attrition, ZnO particles induced the photoactivation of hydroxyapatite by creating defect sites in the crystal lattice; therefore, the composite samples CHZ3 with 75% HA content, after 4 h of UV irradiation, exhibited a similar photocatalytic effect (0.017×10^{-5} mg/L) as CHZ3, having 75% ZnO content (0.050×10^{-5} mg/L) and CHZ5 (0.086×10^{-5} mg/L), but placed in opposition with CHZ2 (100% HA). However, the CHZ2 sample showed weak photocatalytic properties, and the remanent MO concentration slowly decreased from 5.04×10^{-5} mg/L, after 30 min of dark contact with dye solution, to 4.27×10^{-5} mg/L after 4 h of UV irradiation. This fact can be explained by the ion exchange properties of HA on the vulnerable Ca^{2+} and $(PO_4)^{3-}$ positions and retention in the crystalline structure of MO by attracting cationic (Na^+) or anionic (SO_3^{2-}) groups from methyl orange molecules. Also, the defect site in the crystal lattice generated by the coprecipitation synthesis method without subsequent annealing step led to a low crystallinity degree and a less structured crystal lattice, as observed in the XRD plots. The results recommend the obtained composites as advanced materials for utilization in wastewater treatment against dye-type organic pollutants.

Author Contributions: Conceptualization, C.R.D. and F.-D.G.; methodology, E.H.; formal analysis, L.-M.Ș.; investigation, F.-D.G.; resources, M.M.; writing—original draft preparation, F.-D.G. and L.-M.Ș.; writing—review and editing, C.R.D.; visualization, E.H.; supervision, M.M.; funding acquisition, F.-D.G. All authors have read and agreed to the published version of the manuscript.

Funding: This research was funded by the Ministry of Research, Innovation and Digitalization from Romania, contract no. 44N/2023.

Institutional Review Board Statement: Not applicable.

Informed Consent Statement: Not applicable.

Data Availability Statement: Data are available in this manuscript.

Acknowledgments: This work was carried out through the Core Program BIO-CliMission of the National Plan for Research, Development and Innovation 2022–2027, and with the support of MCID, project no. PN 23 31 03 01.

Conflicts of Interest: The authors declare no conflicts of interest.

References

1. Supin, K.K.; Namboothiri, M.P.P.; Vasundhara, M. Enhanced photocatalytic activity in ZnO nanoparticles developed using novel Lepidagathis ananthapuramensis leaf extract. *RSC Adv.* **2023**, *13*, 1497–1515.
2. Xian, B.C.C.; Kang, C.W.; Wahab, M.A.; Zainol, M.R.R.M.A.; Baharudin, F. Evaluation of low impact development and best management practices on peak flow reduction using SWMM. *IOP Conf. Ser. Earth Environ. Sci* **2021**, *646*, 012045. [CrossRef]
3. Ramli, N.; Hamid, H.A.; Yahaya, A.S.; Ul-Saufie, A.Z.; Noor, N.M.; Seman NA, A.; Kamarudzaman, A.N.; Deák, G. Performance of Bayesian Model Averaging (BMA) for Short-Term Prediction of PM10 Concentration in the Peninsular Malaysia. *Atmosphere* **2023**, *14*, 311. [CrossRef]
4. Ilie, M.; Deák, G.; Marinescu, F.; Ghita, G.; Tociu, C.; Matei, M.; Covaliu, C.I.; Raischi, M.; Yusof, S.Y. Detection of Emerging Pollutants Oxytetracycline and Paracetamol and the Potential Aquatic Ecological Risk Associated with their Presence in Surface Waters of the Arges-Vedea, Buzau-Ialomita, Dobrogea-Litoral River Basins in Romania. *IOP Conf. Ser. Earth Environ. Sci.* **2020**, *616*, 012016. [CrossRef]
5. Maria, C.; Deák, G.; Tudor, G.; Holban, E.; Zamfir, C.; Ivanov, A.A.; Grigore, G.; Rahim, N. Investigation of Microplastics Presence in the Dambovita River. *Int. J. Conserv. Sci.* **2023**, *14*, 663–670. [CrossRef]
6. Doicin, I.E.; Preda, M.D.; Neacsu, I.A.; Ene, V.L.; Birca, A.C.; Vasile, B.S.; Andronescu, E. Tailoring Zinc Oxide Nanoparticles via Microwave-Assisted Hydrothermal Synthesis for Enhanced Antibacterial Properties. *Appl. Sci.* **2024**, *14*, 7854. [CrossRef]
7. Daescu, A.; Holban, E.; Boboc, M.; Raischi, M.; Matei, M.; Ilie, M.; Deak, G.; Daescu, V. Performant technology to remove organic and inorganic pollutants from wastewaters. *J Environ. Prot. Ecol.* **2017**, *18*, 304–312.
8. Jihane Labrag, E.B.; Oulguidoum, A.; Robert, D.; Laghzizil, A.; Nunzi, J.M. Porous and Bifunctional ZnO-Hydroxyapatite Nanostructure for Photocatalytic Degradation of Paracetamol and Methylene Blue in Water. *Iran. J. Catal.* **2021**, *11*, 389–395.
9. Rayaroth, M.P.; Aravindakumar, C.T.; Shah, N.S.; Boczkaj, G. Advanced oxidation processes (AOPs) based wastewater treatment—Unexpected nitration side reactions—A serious environmental issue: A review. *Chem. Eng. J.* **2022**, *430*, 133002. [CrossRef]
10. Loddo, V.; Bellardita, M.; Camera-Roda, G.; Parrino, F.; Palmisano, L. Chapter 1—Heterogeneous Photocatalysis: A Promising Advanced Oxidation Process. In *Current Trends and Future Developments on (Bio) Membranes*; Basile, A., Mozia, S., Molinari, R., Eds.; Elsevier: Amsterdam, The Netherlands, 2018; pp. 1–43.
11. Burlacu, I.F.; Deák, G.; Marcu, E.; Serre, I.P.; Balloy, D.; Halin, D.S.C. Photocatalytic degradation of a refractory water pollutant using nanosized catalysts. *J. Environ. Prot. Ecol.* **2020**, *21*, 571–578.
12. Lindino, C.A.; Batalioto, C.F.; Hoss, D.; Schuranck, S.C.H. Degradação do Agrotóxico Connect® com Fotocatalisador Hidroxiapatita. *Ciência Nat.* **2016**, *38*, 1570–1579. [CrossRef]
13. Burdusel, A.C.; Neacsu, I.A.; Birca, A.C.; Chircov, C.; Grumezescu, A.M.; Holban, A.M.; Curutiu, C.; Ditu, L.M.; Stan, M.; Andronescu, E. Microwave-Assisted Hydrothermal Treatment of Multifunctional Substituted Hydroxyapatite with Prospective Applications in Bone Regeneration. *J. Funct. Biomater.* **2023**, *14*, 378. [CrossRef]
14. Reddy, M.; Venugopal, A.; Subrahmanyam, M. Hydroxyapatite photocatalytic degradation of calmagite (an azo dye) in aqueous suspension. *Appl. Catal. B Environ.* **2007**, *69*, 164–170. [CrossRef]
15. Corami, A.; Mignardi, S.; Ferrini, V. Cadmium removal from single- and multi-metal (Cd + Pb + Zn + Cu) solutions by sorption on hydroxyapatite. *J. Colloid Interface Sci.* **2008**, *317*, 402–408. [CrossRef]
16. Gatou, M.A.; Kontoliou, K.; Volla, E.; Karachalios, K.; Raptopoulos, G.; Paraskevopoulou, P.; Lagopati, N.; Pavlatou, E.A. Optimization of ZnO Nanoparticles' Synthesis via Precipitation Method Applying Taguchi Robust Design. *Catalysts* **2023**, *13*, 1367. [CrossRef]
17. Burlacu, I.F.; Favier, L.; Matei, E.; Predescu, C.; Deák, G. Successful elimination of a refractory emergent organic compound from aqueous system using different catalytic materials. *UPB Sci. Bull.* **2019**, *81*, 217–225.
18. El Bekkali, C.; Bouyarmane, H.; El Karbane, M.; Masse, S.; Saoiabi, A.; Coradin, T.; Laghzizil, A. Zinc oxide-hydroxyapatite nanocomposite photocatalysts for the degradation of ciprofloxacin and ofloxacin antibiotics. *Coll. Surf. A Colloid Surf. A Physicochem. Eng. Asp.* **2018**, *539*, 364–370. [CrossRef]
19. Kugarajah, V.; Hadem, H.; Ojha, A.K.; Ranjan, S.; Dasgupta, N.; Mishra, B.N.; Dharmalingam, S. Chapter 1—Fabrication of nanomaterials. In *Food, Medical, and Environmental Applications of Nanomaterials*; Pal, K., Sarkar, A., Sarkar, P., Bandara, N., Jegatheesan, V., Eds.; Elsevier: Amsterdam, The Netherlands, 2022; pp. 1–39.

20. Tanji, K.; Navio, J.A.; Chaqroune, A.; Naja, J.; Puga, F.; Hidalgo, M.C.; Kherbeche, A. Fast photodegradation of rhodamine B and caffeine using ZnO-hydroxyapatite composites under UV-light illumination. *Catal. Today* **2022**, *388–389*, 176–186. [CrossRef]
21. Dumitrescu, C.R.; Neacsu, I.A.; Surdu, V.A.; Nicoara, A.I.; Codrea, C.I.; Pop, C.E.; Trusca, R.; Andronescu, E. Maturation of Hydroxyapatite from Biogenic Calcium Source—A Comparative Study. *UPB. Sci. Bull. Ser. B* **2022**, *84*, 19–30.
22. Deák, G.; Dumitru, F.D.; Moncea, M.A.; Panait, A.M.; Baraitaru, A.G.; Olteanu, M.V.; Boboc, M.G.; Stanciu, S. Synthesis of ZnO nanoparticles for water treatment applications. *Int. J. Conserv. Sci.* **2019**, *10*, 343–350.
23. Walters, C.; Keeney, A.; Wigal, C.; Johnson, C.; Cornelius, R. The Spectrophotometric Analysis and Modeling of Sunscreens. *J. Chem. Educ.* **1997**, *74*, 99. [CrossRef]
24. Sheng, G.; Qiao, L.; Mou, Y. Enhanced activity of silver modified thin-film TiO_2 photocatalysts. *J. Environ. Eng.* **2011**, *137*, 611–616. [CrossRef]